

# Plug flow and the breakdown of Bagnold scaling in cohesive granular flows

Robert Brewster,<sup>1</sup> Gary S. Grest,<sup>2</sup> James W. Landry,<sup>3</sup> and Alex J. Levine<sup>1</sup>

<sup>1</sup>*Department of Chemistry and Biochemistry,  
UCLA, Los Angeles, CA 90095-1596*

<sup>2</sup>*Sandia National Laboratories, Albuquerque NM 87185*

<sup>3</sup>*BAE Systems Burlington, MA 01803*

(Dated: May 6, 2019)

Cohesive granular media flowing down an inclined plane are studied by discrete element simulations. Previous work on *cohesionless* granular media demonstrated that within the steady flow regime where gravitational energy is balanced by dissipation arising from intergrain forces, the velocity profile in the flow direction scales with depth in a manner consistent with the predictions of Bagnold. Here we demonstrate that this Bagnold scaling does not hold for the analogous steady-flows in cohesive granular media. We develop a generalization of the Bagnold constitutive relation to account for our observation and speculate as to the underlying physical mechanisms responsible for the different constitutive laws for cohesive and noncohesive granular media.

PACS numbers: 45.70.-n, 45.70.Mg, 83.10.Ff

## I. INTRODUCTION

One of the central questions in the study of granular flows is how to determine the relationship between the microphysics of grain interactions and the collective or macroscopic flow properties of the system. Elucidating these flow properties is of fundamental importance to a variety of fields ranging from civil engineering to geophysics [1]. Moreover, this question remains at the forefront of many-body physics as its solution appears to demand entirely new concepts that are applicable to systems driven far from equilibrium.

In this article we explore the velocity field in steadily flowing granular media in the chute geometry – an inclined plane having a rough surface at its base and a free surface at the top. Such flows have been previously characterized both experimentally [2, 3, 4, 5, 6, 7, 8, 9] and via simulation [10, 11, 12, 13, 14, 15, 16]. In this work we address, through large-scale discrete element simulations, the change in the flow field in the material as a function of interparticle adhesion. We present a modified constitutive law relating shear stress within the bulk to the local gradients in the velocity field and discuss the implications of our proposed continuum description of the material. In addition we observe the formation of a plug flow regime in the cohesive slab extending from the free surface at the top of the slab into the bulk. The depth of this plug flow regime can be calculated from a comparison of the yield stress of the cohesive material to depth-dependent shear stress due to the weight of the slab.

The study of cohesive granular media is necessary for the application of granular physics to the behavior of such materials in their geophysical context, *i.e.* the dynamics of landslides, snow avalanches, and even the lunar regolith. In the former examples, a small aqueous wetting layer on the particles forms menisci at intergrain contacts to produce an adhesive force. In the latter case, high-vacuum conditions facilitate close contacts between

particles leading to interparticle adhesion due to van der Waals interactions. The study of cohesive granular materials also helps to elucidate fundamental questions concerning the physical description of this state of matter. One aspect of granular materials that differentiates them from random elastic solids or liquids is that cohesionless granular system cannot support tensile stresses. By observing the quantitative effect of known cohesive forces upon granular flows, one should be able to bridge between the better understood elastic solids and/or viscous liquids and granular materials, which, by comparison, remain rather mysterious. The change in the stress-strain relation due to internal cohesion also provides insight into the rheology of cohesionless granular matter. We discuss this further below.

In the study of granular mechanics it is clearly desirable to develop a continuum description of flow since calculating the detailed dynamics of numerous intergrain collisions rapidly becomes intractable with increasing numbers of such particles. In addition one expects, based on experience with the continuum mechanics of solids, liquids, and gases, to be able to develop a set of relations between macroscopic averaged observable such as the velocity field  $v_\alpha(\mathbf{x})$ , mass density  $\rho(\mathbf{x})$ , and stress tensor  $\sigma_{\alpha\beta}(\mathbf{x})$  within the steadily-flowing granular material where details of the grain interactions enter through a small set of parameters [17, 18, 19]. Such a constitutive relation between the stress state in the material and its rate of deformation taken together with momentum conservation completely determines the flow properties of the granular system assuming the boundary conditions on the flow are sufficiently well-known. There are now a number of such hydrodynamic descriptions of granular flow which seek to derive such constitutive equations from a more microscopic theory [17, 20]. There are a variety of such models that rely on arguments based on effective viscosities [21, 22, 23], transient force-chains[24] or a superposition of a rate-dependent contribution arising from collisional interactions and a rate-independent

part related to enduring frictional contacts among the grains[25].

A well-known proposal by Bagnold[27] for such a constitutive relation for granular flows is that the shear stress in the flow is proportional to the instantaneous square of the rate of strain tensor and that the density is constant throughout the material. Taking (as we do throughout this work) a coordinate system where the  $x$ -axis is directed in the flow direction and the  $z$ -axis as the upward normal to the inclined plane, the Bagnold relation is

$$\sigma_{xz} = \kappa (\partial_z v_x)^2, \quad (1)$$

where  $\kappa$  is a constant having the dimensions of  $M/L$ . One can reduce the supporting argument for Eq. 1 to dimensional analysis; in the flowing granular system the one energy density available is the kinetic energy of the grains themselves  $\sim \rho v^2$ . As long as the local mass density remains constant, Galilean invariance requires the shear stress to be proportional to the square of the velocity difference across the sample. The further assumption that the relationship between stress and the rate of strain is local produces Eq. 1. A simple heuristic argument to derive the scaling relation shown in Eq. 1 and attributed to Bagnold is as follows: the transport in the gradient direction ( $\hat{z}$ ) of the component of momentum parallel to the velocity direction ( $\hat{x}$ ) occurs only through collisions between grains. The rate of those collisions depends on the average velocity difference between grains at different locations along the gradient direction  $\sim a \partial_z v_x$  where  $a$  is the grain radius. The momentum transfer per collision also scales linearly with the velocity difference leads to  $\sigma_{xz} \sim m(a \partial_z v_x)^2$  where  $m$  is the mass of a single grain.

It is instructive to compare the above argument to the standard expression for the viscosity of a gas as determined by kinetic theory. In that case the rate of intermolecular collisions is controlled by the root mean square velocity of the gas molecules that is fixed by the equipartition theorem. Thus the viscosity of the gas is proportional to the square root of temperature. The granular system is effectively at zero temperature so that the random particle velocities are driven themselves by the macroscopic velocity scale making the effective granular viscosity as extracted from Eq. 1 depend on shear rate.

In the remainder of this article we first discuss the simulation method in section II before turning to a discussion of our numerical results and calculations in section III. In that section we discuss the effect of intergrain adhesion on the validity of the Bagnold constitutive law. We then conclude in section IV.

## II. SIMULATION METHOD

We performed discrete element simulations on a three-dimensional system of  $N$  monodisperse particles of mass  $m$  and diameter  $d$  on a rough base tilted an angle  $\theta$  with respect to gravity. Our simulations volume is a rectangular box with periodic boundary conditions in both the



FIG. 1: (color online) A representative example of the flowing granular slab of height  $H = 300$ . In this cohesive granular slab ( $A = 0.8$ ) the system separates into a solid-like plug (blue) sliding upon a flowing granular bed (red). The rough surface of inclined plane is shown in green.

$x$  and  $y$  directions, a rough base and an open top. The rough base is created by taking a slice through a previously random close packed state of particles with the same diameter  $d$ . We define the  $z$ -axis to be normal to the base and the  $x$ -axis as the direction of flow. We study a system of length  $40d$  and  $10d$  in the  $x$  and  $y$  directions respectively. We studied three granular slabs of differing heights  $H$ , containing 42000, 83000, and 125000 particles respectively. We refer to these three systems by their approximate height, namely  $H = 100d$ ,  $200d$ , and  $300d$ . We show an example of a cohesive granular material in the steadily flowing state in Fig. 1 for  $H = 300d$ .

We employ a modified version of the model developed by Cundall and Strack [28] to model cohesionless particulates. The model uses Hookean contacts to model grain to grain interactions. We add a cohesive force between particles to simulate damp granular media. Two contacting spheres  $i$  and  $j$  with positions  $\mathbf{r}_i$  and  $\mathbf{r}_j$  are separated by  $\mathbf{r}_{ij} = \mathbf{r}_i - \mathbf{r}_j$ , the compression is then  $\delta_{ij} = d - |\mathbf{r}_{ij}|$ . The relative velocity is  $\mathbf{v}_{ij} = \mathbf{v}_i - \mathbf{v}_j$  which can be separated into normal and tangential components

$$\mathbf{v}_{n_{ij}} = (\mathbf{v}_{ij} \cdot \mathbf{n}_{ij}) \mathbf{n}_{ij} \quad (2)$$

$$\mathbf{v}_{t_{ij}} = \mathbf{v}_{ij} - \mathbf{v}_{n_{ij}} - \frac{1}{2}(\omega_i + \omega_j) \times \mathbf{r}_{ij}. \quad (3)$$

The normal and tangential forces acting on particle  $i$  due to particle  $j$  can then be written as

$$\mathbf{F}_{n_{ij}} = (k_n \delta_{ij} \mathbf{n}_{ij} - \frac{m}{2} \gamma_n \mathbf{v}_{n_{ij}}) + \mathbf{F}_{ij}^c(\delta_{ij}) \quad (4)$$

$$\mathbf{F}_{t_{ij}} = (-k_t \mathbf{u}_{t_{ij}} - \frac{m}{2} \gamma_t \mathbf{v}_{t_{ij}}), \quad (5)$$

where  $k_n, k_t$  and  $\gamma_n, \gamma_t$  are the elastic and viscoelastic constants for interparticle motion along ( $n$ ) and normal to the line of centers ( $t$ ).  $\mathbf{u}_{t_{ij}}$  is the elastic tangential displacement that is set equal to zero at the initiation of contact and is truncated to satisfy the Coulomb yield criterion,  $|\mathbf{F}_{t_{ij}}| < \mu|\mathbf{F}_{n_{ij}}|$ . The additional normal force  $\mathbf{F}_{ij}^c(\delta_{ij})$ , is the cohesive normal force between particles  $i$  and  $j$ . This normal force is derived from an effective cohesive potential acting on particle  $i$  due to particle  $j$ . We simply choose a gaussian well centered around particle  $j$

$$U_{ij}^c = -Ae^{-\frac{\delta_{ij}^2}{\ell^2}}, \quad (6)$$

where  $A$  is the strength of the attraction (in units of mgd) and  $\ell$  is the width of the well. The force is then  $\mathbf{F}_{ij}^c = -\nabla U_{ij}^c$ . We focus on  $0.0 \leq A \leq 1.0$ , where  $A = 1.0$  corresponds to a force capable of supporting 85 particles under gravity. While this form of the cohesive potential cannot be justified in terms of details of either van der Waals or wetting-layer mediated interparticle interactions, we choose this form so that we can vary the strength of the interparticle cohesion via the well depth  $A$  while maintaining the short-range nature of the interaction, which is controlled by  $\ell$ . The force captures the essential features of more physical adhesion scenarios and we expect that the effects of interaction cohesion as modelled here, to accurately reflect the behavior of experimentally accessible cohesive granular media.

Most of the simulations were run with  $k_n = 2 \times 10^5 \frac{mg}{d}$ ,  $k_t = \frac{2}{7}k_n$ ,  $\gamma_n = 50\tau^{-1}$ , and  $\gamma_t = 0$ , where  $\tau = \sqrt{d/g}$ . For the case of Hookean springs used here, these parameters give a coefficient of restitution  $e_n = 0.88$  for normal collisions. The normal spring constant  $k_n$  is large enough to minimize the overlap between particles but small enough to be computationally efficient. Previous simulations for cohesionless grains [14] found that this value of  $k_n$  provides results similar to those for larger values of  $k_n$ . However we do find a subtle dependence of the flow rheology upon the value of  $k_n$  which we explore later in this article. For the coefficient of friction, we use  $\mu = 0.5$ , which is typical for the types of materials we are modeling. The normal damping term operates only when the particles are in actual contact so that, in a narrow window of interparticle separations  $d < r < d + \ell$  these particles will experience a cohesive force without the velocity dependent damping. Interpreted in terms of action of interparticle wetting layers, this suggests that we discount dissipative hydrodynamics in the wetting layer over microscopic plastic deformation in the particle themselves. We expect that such hydrodynamic effects modify the effective value of  $\gamma_n$  as well as the interparticle separation over which it operates, but we have not attempted to model this particular cohesion scenario in detail.

In a gravitational field  $\mathbf{g}$ , the total force on a particle from Eqs. 4, 5, and 6:

$$\mathbf{F}_i^{tot} = m_i \mathbf{g} + \sum_j (\mathbf{F}_{n_{ij}} + \mathbf{F}_{t_{ij}} + \mathbf{F}_{ij}^c), \quad (7)$$

where the sum is over neighboring particles.

The stress tensor within a volume  $V$  is computed by summing over both the contact and kinetic terms of each particle within that volume

$$\sigma_{\alpha\beta} = \frac{1}{V} \sum_i \left[ \sum_{i \neq j} \frac{r_{ij}^\alpha F_{ij}^\beta}{2} + m_i (v_i^\alpha - \bar{v}^\alpha)(v_i^\beta - \bar{v}^\beta) \right], \quad (8)$$

where  $\mathbf{F}_{ij}^\beta = \mathbf{F}_{t_{ij}}^\beta + \mathbf{F}_{n_{ij}}^\beta + \mathbf{F}_{ij}^{c\beta}$  and  $\bar{v}$  is the time-averaged velocity of the particles in  $V$ .

The timestep for the integration of the equations of motion is  $\delta t = 10^{-4}\tau$ . After equilibration the systems were typically run between  $1 - 5 \times 10^7$  time steps. Steady state was determined using the total kinetic energy of the system as a criterion for suitable equilibration of each sample.

### III. RESULTS

In chute flow there are three qualitatively distinct regimes determined by the height of the slab  $H$ , the inclination angle  $\theta$  of the lower surface with respect to the direction of gravity [6, 14], and the intergrain cohesive stresses determined in our model by  $A$  – see Eq. 6. For small enough inclination angles (*i.e.* below the maximum critical angle) or alternatively for short and/or cohesive slabs, the granular heap is stationary. Below the angle of repose for a given slab height and cohesive energy, transiently flowing states of the slab dissipate energy more rapidly than the input of gravitational potential energy so that the slab stops. We refer to this as the no flow regime. At much larger angles, on the other hand, the energy dissipation with the slab is less than the gravitational energy input so that the slab continuously accelerates down the plane. We refer to the parameter space exhibiting this behavior as the unstable regime. At angles intermediate between these two regimes for a given cohesive energy and slab height, we observe steady-state flows. In this work we concentrate primarily on such steady-state behavior in slabs of the largest height  $H = 300d$ . The phase diagram spanned by the cohesion parameter  $A$  and the inclination angle of the slab  $\theta$  for this system shown in Fig. 2. In this work we investigate the steady-state flowing regime after transient behavior associated with the initiation of flow have decayed. The onset of such steady-state behavior is determined by observing the total kinetic energy of the system.

#### A. Plug-flow

In Fig. 3a we plot the velocity in the flow direction vs. height from the bottom of the slab ( $z$ ) for a range of values of the cohesive energy  $A$ . In each case the inclination angle is  $\theta = 22^\circ$ . One of the central results of this work is immediately evident in these figures. For nonzero values

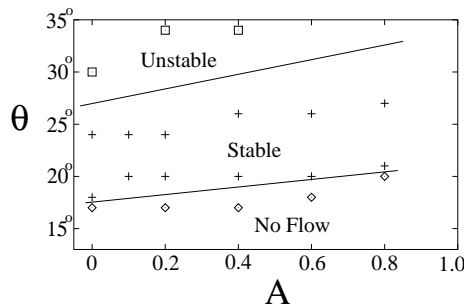


FIG. 2: Phase diagram for chute flow of a fixed height granular slab. The diagram is spanned by the tilt angle  $\theta$  and strength of cohesion  $A$ . There exist three well defined regions corresponding to no flow, stable flow and unstable flow. Lines are drawn to separate the regions.

of the intergrain cohesive energy  $A$ , the velocity plateaus at a finite fraction of the height of the slab. The granular material has, in effect, phase separated into a liquid-like flowing region and a solid-like region that does not admit a non-zero rate of the shear strain. We refer to this behavior near the free surface as plug flow and the solid-like region as the plug. It is clear from this figure that the thickness of the plug depends on the cohesive energy  $A$ . Figure 3b shows the dependence on the plug thickness at fixed  $A$  on the inclination angle  $\theta$ . Finally, Fig. 3c demonstrates that the thickness of the plug is independent of the total height of the slab as long as the material remains in the flowing state for that slab height. Therein the granular velocity down the chute for three slabs of heights  $H = 100d$ ,  $200d$ , and  $300d$  is plotted as a function of the depth from the free surface for an inclination angle of  $\theta = 22^\circ$  and  $A = 0.8$ .

The development of the plug in steady state is signalled not only by the appearance of the velocity plateau, but also by the development of the localized jump in the particle volume fraction with height. The flowing material below due to shear dilatancy is generically at a lower volume fraction, while the plug is denser. Typically this volume fraction change is on the order of 4% and occurs over a height range of 4 – 10 particle diameters. We use this abrupt change in the particle volume fraction with height to more precisely determine the interface between the flowing and plug regimes. The inset of Fig. 4 shows a typical example of this volume fraction change at the plug boundary.

To interpret these observations, we propose that the cohesive granular material can support a finite yield stress  $\sigma_c$  before flowing. Since shear flow requires dilatancy, the critical yield stress should be equal to the typical cohesive stress in the pile. We estimate the maximal value of this cohesive stress as follows. We assume all contacts provide some average adhesive force and then calculate the mean number of such interparticle contacts per unit cross-sectional area,  $n_c$ , in terms of the volume fraction of the particles,  $\phi$ . The yield stress is then estimated as the product of the average adhesive force per

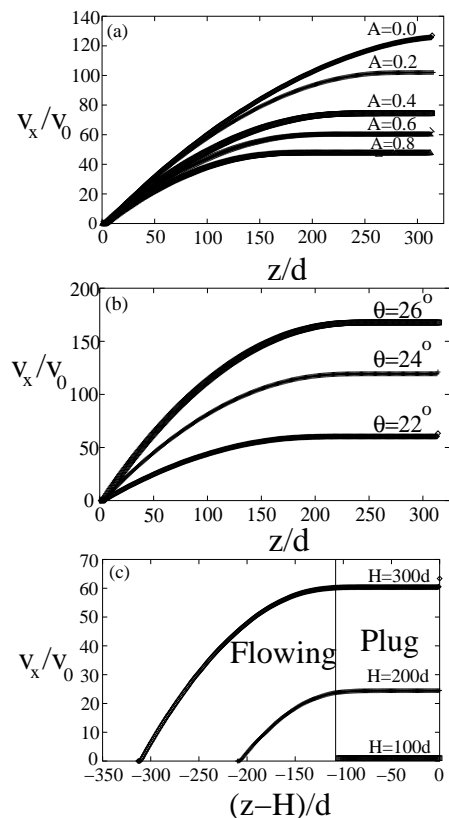


FIG. 3: Velocity profiles as a function of  $z$ . In all three figures the velocity is measured in units of  $v_0 = \sqrt{gd}$ . In (a) profiles are shown for different values of  $A$  with  $\theta = 22^\circ$ ,  $H = 300d$ . In (b) velocity profiles for different values of the tilt angle  $\theta$  with  $A = 0.6$ ,  $H = 300d$ . And (c) the velocity profile as a function of the depth from the free surface for differing slab heights  $H$  with  $A = 0.6$ ,  $\theta = 22^\circ$ . For  $H = 100d$ , only a stopped plug is observed as  $H$  is similar to the size of the plug,  $w$ . In each profile two distinct regions are visible, a flowing state at depth and a plug flow of varying thicknesses at the free surface. For the noncohesive case  $A = 0.0$  the plug size vanishes.

contact and  $n_c$ . To determine the average adhesive force per contact,  $\bar{f}$ , we assume that the interparticle separations at each contact are randomly distributed within the attractive potential well between  $d$  and  $d + \ell$ . Using this assumption we find that the mean magnitude of the adhesive force is given by

$$\bar{f} = \frac{|U(0) - U(\ell)|}{\ell}, \quad (9)$$

in terms of the potential  $U$  defined in Eq. 6. From Eq. 9 and  $n_c = 3\phi/(2\pi a^2)$  we find that the yield stress is

$$\sigma_c = \frac{3\phi\bar{f}}{2\pi a^2}. \quad (10)$$

We determine the thickness of the plug  $w$  by equating the shear stress in the slab due to the weight of the overlying

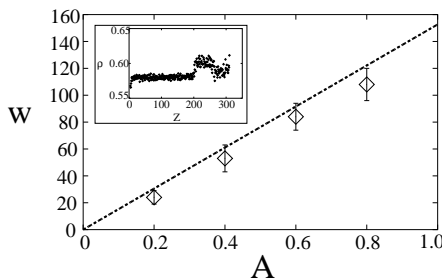


FIG. 4: The thickness of the plug  $w$  vs. the cohesive energy  $A$  for a fixed angle of inclination,  $\theta = 22^\circ$ , and pile height,  $H=300d$ . The dashed line shows the plug width prediction from Eq. 11. The uncertainties in the plug thickness are determined from the width of the density jump at the lower boundary of the plug. Note that the plug boundary becomes more diffuse for smaller values of  $A$ .

material to this yield stress. We find the thickness of the plug is

$$w = \frac{A}{\ell \sin \theta} \left[ \frac{e-1}{e} \right], \quad (11)$$

where  $e$  is the base of the natural logarithm. To test this proposal we plot in Fig. 4 the calculated plug from Eq. 11 with that measured by particle density change at the plug boundary.

Over the parameter range tested, the calculated thickness of the plug is in reasonable agreement with the data. Clearly the linear dependence of the plug size on the cohesive energy is supported by the data. Precise tests of the  $1/\sin \theta$  dependence of the plug thickness, on the other hand, are difficult due to the limited range of available angles for which the slab exhibits steady-state flow. Our calculation of the slope of the theoretical curve must be treated as an upper bound as it is based on the assumption that all interparticle contacts generate some attractive force. Due to jamming in disordered sphere packings, it is reasonable to suppose that at least some contacts have interparticle spacings less than  $d$  and are therefore repulsive in nature. Such contacts between jammed spheres reduce the effective yield stress.

## B. Testing Bagnold-scaling

From the Bagnold conjecture, Eq. 1, for the constitutive relation in the flowing granular state, one may immediately determine the flow profile down the chute. The resulting velocity profile takes the form:

$$v_x(z) = 2\sqrt{\frac{H^3 \rho g \sin \theta}{9\kappa}} \left[ 1 - \left( \frac{H-z}{H} \right)^{3/2} \right]. \quad (12)$$

In Appendix A we derive this velocity profile for the case of a free surface at the top of the flowing medium, *i.e.* no plug as well as the analogous velocity profile for the case

of a finite shear stress applied to the top of the flowing state due to the weight of the plug.

In previous research on cohesionless granular chute flow ( $A = 0.0$ ), the down-chute velocity versus height  $v_x(z)$  has been reported as being consistent with the Bagnold power-law form. We also find such apparently reasonable agreement – see the uppermost curve in Fig. 3a. In the presence of cohesion ( $A > 0$ ), however, the expected Bagnold velocity profile fits the data poorly. We interpret this failure of the Bagnold hypothesis as demonstrating a new mode for vertically transporting ( $z$ ) down-chute momentum ( $p_x$ ) due to the presence of long-lived contacts in the material. These long-lived adhesive contacts in the material create clusters spanning different streamlines in the flow as has been proposed by Ertaş and Halsey [29]. In the presence of shearing flow, these forces acting along these clusters of particles transmit momentum  $p_x$  proportional to the shear rate  $\dot{\gamma} = \partial v_x / \partial z$ . Thus, for cohesive granular materials the Bagnold relation can be generalized to a form that is a sum of terms that are linear and quadratic in the shear rate. We propose the modified Bagnold relation,

$$\sigma_{xz} - \sigma_c = \kappa \left( \frac{\partial v_x}{\partial z} \right)^2 + \beta \left( \frac{\partial v_x}{\partial z} \right). \quad (13)$$

The second of these terms represents the new mode of momentum transport made possible through the long-lived contact networks in the material while the first term arises from the short time scale collisions originally considered by Bagnold [27]. The constant stress term on the LHS of the above equation is the finite yield stress of the cohesive material. The above relation applies only in the flowing states, *i.e.* for values of the shear stress greater than the yield stress  $\sigma_c$ . The constant  $\kappa$  is the Bagnold parameter introduced earlier in Eq. 1, while the second constant  $\beta$ , having dimensions of a viscosity measures the relative importance of the long-lived contacts to the transient collisions. Clearly, this modified constitutive relation leads to a new velocity profile  $v_x(z)$  for the material below the plug. In Fig. 5 we plot two best fits to the velocity profile in the flowing state. We have chosen data corresponding to  $A = 0.8$ ,  $\theta = 22^\circ$  that shows a typical example of the flow profile in the strongly cohesive limit. The curve (+) is the fit of the data to the Bagnold velocity profile where we have used the least-squares method. Note that one cannot simultaneously fit this initial slope of the velocity profile and match the curvature of the data. The modified Bagnold relation gives the best fit to the data.

Simply demonstrating a better fit with the modified Bagnold form is not, in itself, conclusive evidence of the breakdown of Bagnold scaling as one expects a better fit from a model with an extra adjustable parameter. To better justify our conjecture we first examine the dimensionless ratio of the viscous stress proportional to  $\beta \dot{\gamma}$  to the Bagnold stress,  $\kappa \dot{\gamma}^2$ :

$$\Omega = \frac{\beta}{\kappa \dot{\gamma}}. \quad (14)$$

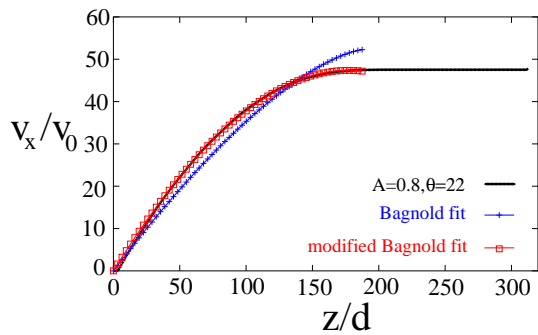


FIG. 5: (color online) Velocity profile for  $A = 0.8$ ,  $\theta = 22^\circ$  showing the difference in the standard Bagnold fit (blue +) and the modified Bagnold fit (red  $\square$ ).

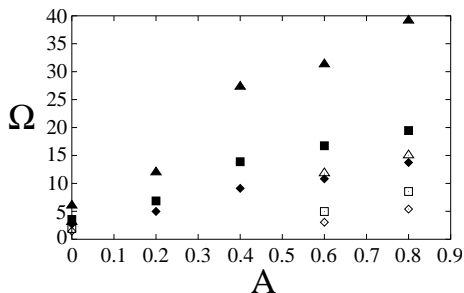


FIG. 6:  $\Omega$  vs  $A$  for  $\theta = 22^\circ$  (closed symbols),  $24^\circ$  (open symbols) at three different heights in the flowing slab ( $\diamond$  for  $z = H/4$ ,  $\square$  for  $z = H/2$ , and  $\triangle$  for  $z = 3H/4$ ).  $\Omega$  is a measure of the importance of the linear term in  $\sigma_{xz}$ , as  $A$  increases so does the importance of this linear term

For the Bagnold hypothesis,  $\Omega$  vanishes. In essence we can determine the extent of the breakdown of such Bagnold scaling by extracting the fit parameters  $\kappa, \beta$ , as well as the shear rate from velocity profiles as shown in Fig. 5 in order to compute the value of  $\Omega$  from our numerical data. This ratio can be computed for a variety of samples having different tilt angle and different cohesive energies. In addition the ratio can be computed at different heights within the flowing layer of a given sample.

In Fig. 6, we show a plot of  $\Omega$  vs.  $A$ . Examination of this figure reveals three trends. First, we note that for any height  $z$  within the flowing part of the slab and for any tilt angle  $\theta$ ,  $\Omega$  increases with increasing cohesive energy  $A$ . The deviation for a purely Bagnold constitutive law as measured by  $\Omega$  increases with height in the slab for all measured angles and cohesive energies. For a given height in the slab and a given cohesive energy one finds that  $\Omega$  decreases within increasing tilt angle  $\theta$ .

The increase of  $\Omega$  with  $A$  for all heights and angles strongly suggests that the internal cohesion is primarily responsible for the breakdown of the Bagnold scaling. That the magnitude of the discrepancy between the observed flows and those derived from the Bagnold hypothesis depends on the height within the slab ( $\Omega$  vs.  $z$  at fixed  $A$  and  $\theta$ ) is consistent with our hypothesis that long-lived contacts cause this discrepancy. Clearly as one ap-

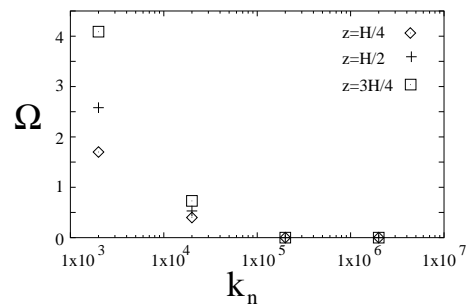


FIG. 7:  $\Omega$  vs  $k_n$  for cohesionless granular flows for  $H = 100d$  and  $\theta = 22^\circ$ . Note that the Bagnold constitutive law ( $\Omega = 0$ ) describes the data better as the stiffness of the particles increases.

proaches the plug the intergrain contacts have extremely long life-times and the constitutive relation for the material most greatly deviates from the Bagnold form. It is reasonable to suppose that in the region directly below the plug where the gravitational shear stress is only slightly greater than the yield stress of the material that there would be the greatest density of long-lived contacts in the flowing state. Thus, one would expect the greatest deviation from Bagnold scaling near the plug. The data clearly support this; for all tilt angles and cohesive energies  $\Omega$  increases with height in the slab. Finally, as the tilt angle is increased at constant cohesive energy, the total kinetic energy of the system is increased. The grains, having higher typical velocities will now have fewer long-lived contacts and transient forces associated with brief intergrain collisions will become the more dominant momentum-transfer process in the material. Thus the effective constituent law will appear to be closer to the Bagnold form.

It is apparent from Fig. 6 that even in the limit of no cohesion there remains a significant deviation from the original Bagnold constitutive law. This residual discrepancy can be well accounted for by slight interpenetrability of the particles in the simulation. The Bagnold constitutive relation can hold exactly only in the limit of hard sphere particles [30]. To test this point we have examined cohesionless particles of varying stiffness  $k_n$  for  $H = 100d$ . The data in Fig. 7 shows that the residual deviations from Bagnold behavior of our cohesionless model granular material can be attributed to the finite stiffness of the constituent particles.

To more directly test that the breakdown of the Bagnold constitutive relation is due to the growth of the number of long-lived contacts in the flowing states with increasing cohesive energy we compiled a contact time histogram. We measured the times over which two particles remained in contact allowing for both rolling and slipping at the contact. Collecting this data for a few representative runs having either no cohesion ( $A = 0$ ) or strong cohesion ( $A = 0.8$ ) we produced two contact time histograms as shown in Fig. 8. Both histograms reflect the contact times in the horizontal slice of the slab be-

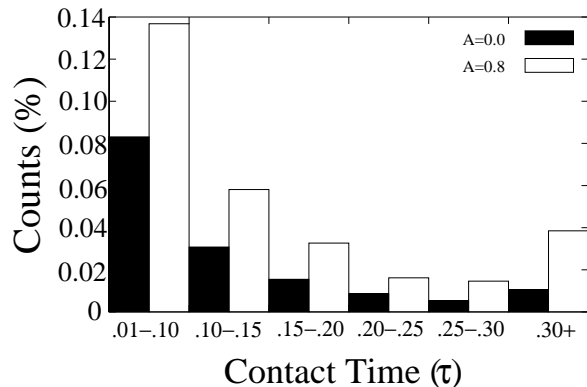


FIG. 8: Contact time histogram within the flowing part of the slab for cohesive energies  $A = 0.0$  (black) and  $A = 0.8$  (blue) with tilt angle  $\theta = 22^\circ$ . The shortest contact time bin has been removed for clarity.

tween  $70 \leq z \leq 100$  over a period of  $10\tau$ . This vertical height was chosen so that it is entirely contained within the flowing regime of the cohesive slab. In fact, from our discussion of Fig. 6, we would expect the largest population of long-lived contacts to be found in the upper part of the flowing region near the plug. For the cohesive system studied using the contact time histogram, we then expect the greatest density of long-time contacts to occur near  $z = 200$ . In both samples the most common contact time is rather short:  $0 < t_{\text{contact}} \leq 0.01\tau$ . This first bin has been removed for clarity. Comparing the two histograms we note that although there are long-lived contacts in both the cohesionless and the cohesive granular material, the number of such contacts is dramatically increased in the cohesive case. As discussed above the presence of long-lived intergrain contacts in the cohesionless case is at least possibly due to the nonzero compressibility of the particles. The enhancement of the number of such long-lived contacts, particularly those having lifetimes greater than  $\sim 0.3\tau$ , with cohesion qualitatively supports our hypothesis that such contacts are primarily responsible for the breakdown of Bagnold scaling in the cohesive granular media. The relationship between this fraction of long-lived contacts and a quantitative model for the parameter  $\beta$  will be explored in a future publication[31].

#### IV. SUMMARY

We have studied the effects of cohesion in steady-state 3D chute flow. Cohesive granular materials generically form two different flow regimes: a solid region (the plug) extending below the free surface characterized by a vanishing shear rate of strain and a flowing region below the plug. The width of this plug region is independent on total depth of the slab but dependent on the tilt angle, cohesive energy, the mass density of the granular material and is accounted for by postulating the appearance

of a finite yield stress in the material. The value of this yield stress can be reasonably determined from estimates of the mean cohesive force within the slab and the mean number of such cohesive contacts.

We find that in the flowing state below the plug the velocity profile is similar to the Bagnold velocity profile:  $v \propto z^{3/2}$ . Nevertheless there remain significant discrepancies between the observed flow profile and the predicted Bagnold form. In light of these deviations from the Bagnold form, we suggest a modified form of the Bagnold constitutive law that combines two essentially independent methods of momentum transfer in the flowing state. This modified Bagnold relation accounts for the usual collisional momentum transfer between grains as well as for momentum transfer due to the cohesive forces acting through the long-term contacts between grains in the flowing state. This modified profile fits the data more closely. Extracting from these fits to the data the ratio of the stress transferred via each method, we find that this ratio exhibits a few reasonable trends. The effect of the long-term contacts grow with cohesive energy and within a single slab as one approaches the plug. This ratio decreases with larger tilt angles; faster flowing slabs should more efficiently break-up any long-lived particle clusters.

To further test this hypothesis we directly measured a contact time histogram within the flowing part of the slab. A comparison between noncohesive and cohesive systems indeed shows a larger number of long-time contacts in the cohesive system. This result qualitatively supports our hypothesis that these contacts are responsible for the breakdown of the Bagnold constitutive law. To provide a true quantitative model for the modified Bagnold constitutive law that we propose it is necessary to calculate from a more microscopic model the stresses transmitted by these long-lived contacts. In order to do so we must determine the spatial correlations between such contacts. These contacts may, in fact, form spatially correlated clusters or chains that span stream-lines in the flow or perhaps represent randomly distributed pairs of particles (dimers) that remain bound for mesoscopic periods during the flow. Clearly, at a fixed density of such long-lived contacts the stress transmission due to these contacts in the former case would be significantly larger than in the latter [31].

Understanding the constitutive relation of cohesive granular materials is clearly of fundamental importance to the study of granular flows in a geophysical context as well as to the handling of granular materials in industry where small amounts of a wetting fluid create adhesion contacts between the grains. Interestingly, this work suggests that studying granular flows in the presence of small amounts of cohesion allows one to break the expected Bagnold scaling in a controllable and computationally efficient manner. It is clear from this work and others [14, 30] that the non-zero compliance of the grains leads to measurable deviations from the Bagnold scaling; the Bagnold law holds in the limit of hard spheres. Studying significantly less compliant grains, however, is computa-

tional difficult. The further study of cohesive granular materials both analytically and computationally should enable the exploration of granular constitutive laws for physically accessible systems that nearly, but not exactly obey the Bagnold constitutive relation.

### APPENDIX A: DERIVATION OF THE VELOCITY FROM THE BAGNOLD CONSTITUTIVE LAW

Bagnold scaling is derived from a constitutive relation between the shear stress and the strain rate

$$\sigma_{xz} = \kappa \dot{\gamma}^2, \quad (\text{A1})$$

where  $\dot{\gamma} = \frac{\partial v_x(z)}{\partial z}$ . The steady-state Cauchy equation for  $\sigma_{xz}$  is

$$\frac{\partial \sigma_{xz}}{\partial z} = \rho g \sin \theta, \quad (\text{A2})$$

therefore

$$\sigma_{xz}(z) = \rho g \sin \theta (H - z), \quad (\text{A3})$$

where  $H$  is the total height of the slab. Solving for  $v_x(z)$  gives the velocity profile shown in Eq. 12 above.

Modified Bagnold scaling is derived from the same constitutive relation used in deriving traditional Bagnold scaling [Eq. A1] with the addition of a linear term in  $\dot{\gamma}$

$$\sigma_{xz} = \kappa \dot{\gamma}^2 + \beta \dot{\gamma}. \quad (\text{A4})$$

Solving this with the same Cauchy equation from Eq. (A3) results in

$$v_x(z) = \frac{2}{3c\sqrt{\kappa}} \left[ (G^2 + cH)^{3/2} - (G^2 + c(H - z))^{3/2} \right] - Gz, \quad (\text{A5})$$

where  $c = \rho g \sin \theta$  and  $G = \frac{\beta}{2\kappa}$

- 
- [1] O. Pouliquen and F. Chevoir, *Physique* **3**, 163 (2002).
  - [2] A. Suzuki and T. Tanaka, *Ind. Eng. Chem. Fundam.* **10**, 84 (1971).
  - [3] D. A. Augenstein and R. Hogg, *Powd. Tech.* **19**, 205 (1978).
  - [4] T. J. Drake, *J. Geophys. Res.* **95**, 8681 (1990).
  - [5] C. Ancey, P. Coussot, and P. Evesque, *Mech. Cohes-Fric. Matter* **1**, 385 (1996).
  - [6] O. Pouliquen, *Phys. Fluids* **11**, 542 (1999).
  - [7] E. Azanza, F. Chevoir, and P. Moucheron, *J. Fluid Mech.* **400**, 199 (1999).
  - [8] C. Ancey, *Phys. Rev. E* **65**, 011304 (2002).
  - [9] O. Pouliquen, *Phys. Rev. Lett.* **93**, 248001 (2004).
  - [10] O.R. Walton, *Mech. Mater.* **16**, 239 (1993).
  - [11] X.M. Zheng and J.M. Hill, *Powd. Tech.* **86**, 219 (1996).
  - [12] S. Dippel and D.E. Wolf, *Comp. Phys. Comm.* **121**, 284 (1999).
  - [13] D.M. Hanes and O.R. Walton, *Powder Technol.* **109**, 133 (2000).
  - [14] L.E. Silbert, D. Ertas, G.S. Grest, T.C. Halsey, D. Levine, and S.J. Plimpton, *Phys. Rev. E* **64**, 051302 (2001).
  - [15] L.E. Silbert, G.S. Grest, S.J. Plimpton, and D. Levine, *Phys. Fluids* **14**, 2637 (2002).
  - [16] L.E. Silbert, J.W. Landry, and G.S. Grest, *Phys. Fluids* **15**, 1 (2003).
  - [17] P.K. Haff, *J. Fluid Mech.* **134**, 401 (1983).
  - [18] S.B. Savage, *Advances in Micromechanics of Granular Materials* eds. J.T. Jenkins and M. Satake (Elsevier, New York) (1992).
  - [19] S.B. Savage, *J. Fluid Mech.* **377**, 1 (1998).
  - [20] J.T. Jenkins and S.B. Savage *J. Fluid Mech.* **130**, 187 (1983).
  - [21] W. Losert, L. Bocquet, T.C. Lubensky, and J.P. Gollub, *Phys. Rev. Lett.* **85**, 1428 (2000).
  - [22] L. Bocquet, W. Losert, D. Schalk, T.C. Lubensky, and J.P. Gollub, *Phys. Rev. E* **65**, 011307 (2001).
  - [23] L. Bocquet, J. Errami, and T.C. Lubensky, *Phys. Rev. Lett.* **89**, 184301 (2002).
  - [24] P. Mills, D. Loggia, and M. Tixier, *Eur. Phys. J. E* **1**, 5 (2000).
  - [25] M.Y. Louge, *Phys. Rev. E* **67**, 061303 (2003).
  - [26] M.Z. Bazant, unpublished (2005).
  - [27] R.A. Bagnold, *Proc. R. Soc. London, Ser A* **225**, 49 (1954); **249**, 235 (1956).
  - [28] P.A. Cundall and O.D.L. Strack, *Geotechnique* **29**, 47 (1979).
  - [29] D. Ertas and T.C. Halsey, *Europhys. Lett.* **60**, 931 (2002); T.C. Halsey and D. Ertas, *cond-mat/0506170* (2005).
  - [30] G. Lois, A. Lemaitre, and J.M. Carlson, *cond-mat/0501535* (2005).
  - [31] R. Brewster and A.J. Levine, in preparation (2005).